Published in final edited form as:
J Neurophysiol. 2007 August ; 98(2): 786–793.

Differential Distribution of Kir4.1 in Spinal Cord Astrocytes Suggests Regional Differences in K^+ Homeostasis

M. L. Olsen, **S. L. Campbell**, and **H. Sontheimer**
Department of Neurobiology, Center for Glial Biology in Medicine, University of Alabama, Birmingham, Alabama

Abstract

Neuronal activity in the spinal cord results in extracellular potassium accumulation that is significantly higher in the dorsal horn than in the ventral horn. This is suggestive of differences in K^+ clearance, widely thought to involve diffusional K^+ uptake by astrocytes. We previously identified the inward rectifying K^+ channel Kir4.1 as the major K^+ conductance in spinal cord astrocytes in situ and hence hypothesized that different expression levels of Kir4.1 may account for the observed differences in potassium dynamics in spinal cord. Our results with immunohistochemical staining demonstrated highest Kir4.1 channel expression in the ventral horn and very low levels of Kir4.1 in the apex of the dorsal horn. Western blots from tissue of these two regions similarly confirmed much lower levels of Kir4.1 in the apex of the dorsal horn. Whole cell patch-clamp recordings from astrocytes in rat spinal cord slices also showed a difference in inwardly rectifying currents in these two regions. However, no statistical difference in either fast-inactivating (Ka) or delayed rectifying potassium currents (Kd) was observed, suggesting these differences were specific to Kir currents. Importantly, when astrocytes in each region were challenged with high $[K^+]_o$, astrocytes from the dorsal horn showed significantly smaller (60%) K^+ uptake currents than astrocytes from the ventral horn. Taken together, these data support the conclusion that regional differences in astrocytic expression of Kir4.1 channels result in marked changes in potassium clearance rates in these two regions of the spinal cord.

INTRODUCTION

Typical mammalian brain values of extracellular potassium, $[K^+]_o$, range from 2.6 to 3.8 mM (Sykova 1983). However, these values fluctuate due to K^+ release into the extracellular space during neuronal activity. Because of the small volume of the extracellular space and low baseline levels of $[K^+]_o$, the release of even small amounts of K^+ can lead to dramatic increases in extracellular K^+ concentrations (Van Harreveld and Malhotra 1967). It has been demonstrated in the rat spinal cord that a single stimulus can increase extracellular K^+ by as much as 5 mM (Walton and Chesler 1988). Sustained increases in $[K^+]_o$ above baseline levels leads to hyperexcitability and affects the integrity of synaptic transmission (Walz 2000). Imperatively, several mechanisms are in place that aid in extracellular K^+ clearance including simple diffusion and energy-dependent mechanisms such as glial and neuronal Na^+-K^+ pumps (Amedee et al. 1997; Kofuji and Newman 2004). Additionally, K^+-selective channels, largely in glial cells, assist in K^+ clearance by moving K^+ ions across their membrane when extracellular K^+ concentrations increase. Potassium spatial buffering, as is termed, is thought to redistribute K^+ to surrounding glia cells via gap junctions where it is released at sites of lower $[K^+]_o$. Potassium spatial buffering is an attractive mechanism for K^+ clearance as it is energy efficient and sequesters potassium in the intracellular space. However, energy-

Address for reprint requests and other correspondence: H. Sontheimer, 1719 6th Ave. S., CIRC 425, Birmingham, AL 35294 (E-mail: sontheimer@uab.edu)..

dependent mechanisms of K^+ clearance have been implicated in potassium uptake as well (D'Ambrosio et al. 2002; MacVicar et al. 2002; Ransom et al. 1995; Xiong and Stringer 1999). It is likely that all three mechanisms contribute to some extent to K^+ clearance after neuronal activity.

Glial cell membranes are endowed with K^+ channels perfectly suited for the task of K^+ clearance. Kir4.1, an inwardly rectifying K^+ channel, has garnered much attention. This channel is expressed in glial cells throughout the CNS (Kofuji et al. 2000; Martin-Caraballo and Dryer 2002; Olsen et al. 2006; Poopalasundaram et al. 2000). Kir4.1 channels have a high open probability at rest (Ransom and Sontheimer 1994), therefore contributing to the high K^+ permeability and negative resting membrane potential of astrocytes. Importantly, channel conductance increases with increasing extracellular K^+ (Hagiwara and Takahashi 1974; Newman 1993; Sakmann and Trube 1984), making Kir4.1 ideally suited for K^+ clearance. The channel's significance in the context of extracellular K^+ regulation and its contribution to the hyperpolarized resting membrane potential, a hallmark of mature astrocytes, has been conclusively demonstrated in animals where Kir4.1 has been genetically inactivated. In Kir4.1 knock-out animals, Muller cells (Kofuji et al. 2000), astrocytes of the ventral respiratory group (Neusch et al. 2006), and spinal cord astrocytes (Olsen et al. 2006) lack inwardly rectifying K^+ currents. Furthermore, K^+ uptake, or clearance capabilities, is decreased, the resting membrane potential is depolarized, and input resistance is markedly increased.

In spinal cord, the dynamics of $[K^+]_o$ are well documented (Frankenhauser and Hodgkin 1956; Jendelova and Sykova 1991; Walton and Chesler 1988). Importantly, striking regional differences in K^+ accumulation were seen after neuronal activity (Walton and Chesler 1988). Specifically, neuronal activity in the dorsal horn causes larger increases in $[K^+]_o$ than in the ventral horn. We demonstrate here that Kir4.1 is more prominently expressed in the ventral horn and after K^+ stimulation gives rise to much enhanced uptake currents. Hence changes in the expression of Kir4.1 appear to translate into marked differences in extracellular K^+ homeostasis.

METHODS

Slice preparation

Experiments were performed on either sex of Sprague-Dawley rats and were approved by the University of Alabama Institutional Animal Care and Use Facility. For slice experiments, P12–P20 pups were anesthetized with CO_2 and decapitated, and the spinal cord was removed and placed in ice-cold calcium-free artificial cerebral spinal fluid (ACSF, containing in mM, 116 NaCl, 4.5 KCl, 0.8 $MgCl_2$, 26.2 $NaHCO_3$, 11.1 glucose, and 5.0 HEPES) for 30 s. The cord was then placed in liquid low-melt agar at ~30°C, which was quickly solidified by placing on ice. Sections from the cervical, thoracic, and lumbar regions were cut at 250 μm using a Vibratome 3000 (Ted Pella, Redding, CA) in calcium-free ACSF. Before recording, slices were allowed to recover for ≥1 h at room temperature in calcium-free ACSF, which was continuously bubbled with 5% CO_2-95%O_2.

Slice electrophysiology

Whole cell voltage-clamp recordings were made as described previously (Olsen et al. 2006). Patch pipettes were made from thin-walled (outer diameter 1.5 mm, inner diameter 1.12 mm) borosilicate glass (TW150F-4) WPI, Sarasota, FL) and had resistances of 4 – 6 MΩ. Slices were transferred after the recovery period to either a Zeiss Axiskop FS microscope (Zeiss, Thornwood, NY) or Leica DMLFSA microscope equipped with Nomarski optics; a ×40 water-immersion lens and infrared illumination was used to visualize glia cells. Signals were acquired using an Axopatch 700B (Molecular Devices, Sunnyvale, CA) or a Axopatch 200B amplifier,

both controlled by Clampex 9.0 software via a Digidata 1200B interface (Axon Instruments). Signals were filtered at 2 kHz and digitized at 5 kHz. Data acquisition and storage were conducted with the use of pClamp 9.0 (Axon Instruments). Resting membrane potentials were measured directly from the amplifier in $I = 0$ mode ~1 min after whole cell access was obtained. Where described in the text whole cell capacitance and series resistances were also measured directly from the amplifier, with the upper limit for series resistance being 10 MΩ and series resistance compensation adjusted to 80% to reduce voltage errors. Slices were continuously superfused with ACSF with the addition of 2.0 mM $CaCl_2$.

The standard KCl pipette solution contained (in mM) 145 KCl, 1 $MgCl_2$, 10 EGTA, and 10 HEPES sodium salt, pH adjusted to 7.3 with Tris-base. $CaCl_2$ (0.2 mM) was added to the pipette solution just before recording, resulting in a free calcium concentration of 1.9 nM. In some experiments, biocytin (0.5 mg/ml) was added to the pipette solution for posthoc identification of recorded cells. Cells were continuously superfused at room temperature with oxygenated ACSF containing 2 mM $CaCl_2$. Drugs were added directly to these solutions. Unless stated otherwise, all drugs were purchased from Sigma (St. Louis, MO).

Western blot analysis

Thick spinal cord slices (1–2 mm) were obtained as described in the preceding text and placed in ice-cold ACSF supplemented with protease inhibitors. Slices were cooled to aid in the removal of the white matter. Gray matter tissue from the ventral or dorsal horn from several serial sections of the spinal cord were placed in lysis buffer (100 mM Tris, pH 7.5, 1% SDS supplemented with protease inhibitors). The tissue was mechanically homogenized and then sonicated for 10 s. Tissue homogenates were centrifuged for 5 min at 12,000 *g* at 4°C. Protein quantification was performed on the supernatant using a DC protein assay kit from Bio-Rad (Hercules, CA). Protein was heated to 60°C for 15 min in an equal volume of 2× sample buffer (100 mM Tris, pH 6.8, 10% SDS in Laemmli-sodium dodecylsulfate, 600 mM β-mercaptoethanol). Equal amounts of protein were loaded into each lane of a 4 –20% gradient precast sodium dodecylsulfate polyacrilamide gel electrophoresis (Bio-Rad). Gels were transferred onto PVDF paper (Millipore, Bedford, MA) at 200 mA constant for 2 h at room temperature and membranes were blocked in blocking buffer (5% dried milk, 2%BSA and 2% goat-serum). The Kir4.1antibody was obtained from Alomone (Jeruselum, Israel) and diluted according to the manufacturer's instructions. Blots were incubated for 90 min at room temperature. The membranes were then rinsed three times for 15 min and incubated with horseradish peroxidase-conjugated secondary antibody for 60 min. Blots were once again washed three times for 10 min and developed with enhanced chemiluminesence (Amersham, Arlington Heights, IL) on Hyperfilm (Amersham).

Immunocytochemistry

Animals (P12–20) were killed with a peritoneal injection of ketamine (100 mg/kg) and were perfused with a 4% paraformaldehyde solution for ~15 min. The whole spinal column was removed and stored in 4% paraformaldehyde overnight. After washing in PBS, the cord was removed from the column, 50-μm sections were cut using a Vibratome (Oxford Instruments) from the mid-cervical, thoracic, and lumbar regions. Sections were blocked for 1 h in 10% horse serum and 0.3% Triton-X100 in PBS. Primary antibodies were diluted according to manufacturer's instructions in blocking buffer diluted 1:3 and incubated with slices overnight. Antibodies against GLT-1, GFAP, Neu-N, and MAP2 were obtained from Chemicon (Temecula, CA). We used GFAP as a positive marker for astrocytes, recognizing that GFAP does not label all astrocytes. For this reason, we also chose to label astrocytic membrane with the astrocyte-specific membrane marker GLT-1. The following day, the sections were washed two times with PBS and two times with diluted blocking buffer before incubating with FITC or TRITC-conjugated secondary antibodies obtained from Molecular Probes for 60 min at room

temperature. Slices were then washed two times with diluted blocking buffer and two times with PBS before being mounted onto glass coverslips. Fluorescent images were acquired with a Zeiss Axiovert 200M (München, Germany). To quantify Kir4.1 expression low-magnification (×5) images were imported into the National Institutes of Health imaging software program ImageJ1.37C. Intensity measurements were made in selected regions of interest corresponding to Rexed's Laminae IX (region1), Rexed's Laminae VII (region 2), Rexed's Laminae V (region 3), and Rexed's Laminae I/II (region 4). Comparisons were matched as we were able to visualize all four regions in each image at one time controlling for exposure times within each individual image.

Statistical analysis

Current responses to varied voltage steps and ramps were analyzed and measured in Clampfit (Molecular Devices); the resulting raw data were graphed and plotted in Origin 6.0 (MicroCal, Northampton, MA). Two-tailed *t*-test and Tukey-Kramer Multiple Comparisons Test were performed using Graphpad software (San Diego, CA) and *P* values are reported in the text. Unless otherwise stated, all values are reported as means ± SE with *n* indicating the number of cells sampled.

RESULTS

We set out to investigate the possibility that heterogeneous Kir4.1 expression contributes to variable K^+ clearance rates in the spinal cord. We began these studies by examining Kir4.1 expression in the rat spinal cord. Slices obtained from paraformaldehyde perfused juvenile rats (P12–P20) of cervical, thoracic, and lumbar sections were immunostained with Kir4.1 and glial- and neuronal-specific cell markers. Kir4.1 immunoreactivity in the gray matter exhibited a distinct labeling pattern with highest expression levels in the ventral horn and minimal Kir4.1 immunoreactivity detected in the superficial layers of the dorsal horn (Rexed Lamina I/II, Fig. 1*A*). To better visualize the labeling pattern of Kir4.1, the gray matter is lightly outlined in black. The black arrows identify the ventral horn, which demonstrates the most intense Kir4.1 labeling. In contrast, the white arrows indicate the superficial layers of the dorsal horn that show very little Kir4.1 labeling. We observed this pattern of labeling throughout the spinal cord. Images from the ventral horn demonstrate Kir4.1 immunoreactivity overlapped or co-localized with the astrocytic-specific membrane marker, glutamate transporter 1 (GLT-1, Fig. 1*B*) but not the neuronal marker Neu-N (Fig. 1, *C* and *D*) Map2 or synaptophysin (data not shown) illustrating glial specificity. This specificity in spinal cord glial cells has been demonstrated previously (Kaiser et al. 2006; Neusch et al. 2001; Olsen et al. 2006). Higher-magnification images demonstrate Kir4.1 reactivity in the ventral horn was the most intense in regions surrounding neuronal cell bodies and along axons (arrowheads, Fig. 1*G*) as well as along capillaries (not shown). These data demonstrate marked heterogeneity of Kir4.1 in astrocytes of the spinal cord with highest expression of Kir4.1 in the ventral horn. In an attempt to quantify Kir4.1 in transverse sections of the spinal cord, we investigated 21 low-magnification images in which we were able to visualize both horns in the same image (Fig. 1*E*). We focused on four particular regions Rexed's Laminae IX (region1), Rexed's Laminae VII (region 2), Rexed's Laminae V (region 3), and Rexed's Laminae I/II (region 4). Mean data from 21 images demonstrate significant differences in Kir4.1 expression between Rexed's Laminae 1/II and all other regions of the spinal cord examined ($P < 0.001$, Tukey-Kramer multiple comparisons test, Fig. 1*F*). Kir 4.1 expression in region 3 or Rexed's Laminae V is also significantly different from Rexed's Laminae 9 ($n = 21$, $P < 0.001$). These data suggest that Kir4.1 exhibits a gradient of immunoreactivity in neonatal rat spinal cord.

We next examined Kir4.1 expression in the dorsal and ventral horn by Western blot analysis. Gray matter tissue from the ventral or dorsal horn from thick (1–2 mm) spinal cord slices was

used to make lysates for Western blotting. Equal amounts of protein were loaded onto a gel and blots from both regions were probed with Kir4.1. We were able to detect bands at ~50 and 200 kD corresponding to a monomer and tetramer of Kir4.1 (Fig. 2). Consistent with the immunohistochemistry results, less Kir4.1 immunoreactivity was detected in the dorsal lanes from two P16 rats. Re-probing the same blot with two astrocytic markers GLT-1 and GFAP indicate that astrocytic number or percentage of astrocytic membrane/milligram of total protein were the same in the dorsal and ventral regions; indeed GLT-1 expression appears slightly higher in the dorsal regions. Hence the differences in Kir4.1 expression cannot be due to an overall difference in astrocyte number in these two regions. To demonstrate that equal concentrations of protein were loaded, this blot was probed with actin. Human embryonic kidney (HEK) cells, which do not express Kir4.1, served as a negative control. We presume the band at ~100 kD to be nonspecific binding as it is also present in the HEK cell lane.

In an attempt to further correlate Kir4.1 protein expression in spinal cord slices with measurable currents, we next performed whole cell, patch-clamp recording on spinal cord slices. Figure 3 shows representative recordings obtained from astrocytes recorded in the ventral horn relative to an astrocytes from the apex of the dorsal horn (Fig. 3*A*). Kir currents were isolated by application of 100 μM Ba^{2+}, a concentration that selectively inhibits currents mediated by Kir4.1 channels. These recordings confirm a greater than twofold difference in the magnitude of the Ba^{2+}-sensitive Kir current. Whole cell currents from both regions maintain a similar profile, namely, inactivation at hyperpolarized potentials, weak rectification and complete inhibition by 100 μM Ba^{2+}. Analysis of responses to a −140-mV step demonstrated a significant difference in Kir amplitude between the two regions with Ba^{2+}-sensitive currents from the dorsal horn being −205.3 ± 44.2 pA (n = 21) and currents from the ventral region measuring −453.8 ± 81.4 pA (n = 25, P = 0.0110; Fig. 3*B*). One might assume cells with larger currents in the ventral horn were more extensively coupled. However, consistent with previously reported data, current amplitude was not dependent on cell coupling (Schools et al. 2006). Of the six cells that were biocytin filled from the ventral horn, only one cell demonstrated significant cell coupling. In the dorsal horn, 8 of the 11 cells visualized by biocytin labeling demonstrated extensive cell coupling. Representative examples of biocytin-filled cells are illustrated in Fig. 3*C*.

To examine whether these differences were specific to inwardly rectifying K^+ currents, we next examined delayed rectifier (Ka) and fast-inactivating (Kd) currents in these same cells. In contrast to the Kir data, there was no statistical difference in either Ka or Kd in the dorsal and ventral horn (Fig. 4). *Panel A* illustrates examples of K^+ channel recordings from two cells, one from each region. The particular examples chosen were identical in size (41 pF), and were obtained from the same animal. The Kir current in the dorsal horn was significantly smaller than Kir currents from the ventral region (Fig. 4*A*, *top*). In these cells, the Ka current in the dorsal cell was larger than that in the ventral horn (Fig. 4*A*, *middle*), whereas the Kd current was similar in magnitude to that in the ventral region (Fig. 4*A*, *bottom*). After examination of >30 cells from the two different regions, however, mean data demonstrate that there is no difference in either Ka or Kd current amplitudes in these two regions. The peak Ka current measured at +100 mV was 2,132.3 ± 225.4 pA, n = 33, in the ventral horn and 2,358.3 ± 199.7 pA, n = 31, in the dorsal horn (Fig. 4*B*). Although the peak Kd current measured at +100 mV was determined to be 1,714.3 ± 179.7 pA, n = 33, in the ventral horn and 1,504.6 ± 161.5 pA, n = 31, in the dorsal horn (Fig. 4*C*). The protocols used to isolate individual currents are shown in Fig. 4*D*.

We next assessed several other electrophysiological properties of astrocytes from the two regions. Previous studies have related Kir channel expression to cell resting membrane potential (V_m); the higher the Kir channel expression, the more hyperpolarized the V_m (Bringmann et al. 1999; Ransom and Sontheimer 1995; Sontheimer et al. 1989; Williamson et

al. 1997). Consistent with these observations, mean data demonstrate astrocytes from the dorsal horn are slightly, but significantly, more depolarized relative to astrocytes from the ventral horn (−67.4 ± 2.4, $n = 33$, and −76.8 ± 1.1, $n = 34$, $P = 0.0008$, Fig. 5*A*). Furthermore, the input resistance (Fig. 5*B*) of cells from the dorsal horn was significantly higher (760.5 ± 171.9, $n = 18$) than astrocytes from the ventral horn (279.1 ± 60.9, $n = 18$, $P = 0.0153$). Kir channels have a high open probability at rest and therefore contribute to the relatively low input resistance seen in astrocytes. The higher input resistance observed in the dorsal horn astrocytes is likely a direct consequence of fewer Kir channels in these astrocytes.

One would expect reduced Kir channel expression would lead to changes in extracellular K^+ dynamics and differences in K^+ uptake currents. To mimic focal increases in K^+, as would be seen after neuronal activity, we pressure applied brief (1, 2, and 3 s) 130 mM K^+ pulses using a Picospritzer taking care to place the K^+-filled electrode at the same distance (~25 μm) from the cell of interest at the same focal plane and using pipette tips with similar diameters. We intentionally placed the puffing pipette very close in proximity and pulsed with saturating concentrations of K^+ to maximize the response in the target cell. Whole cell recordings were used to measure the K^+-induced inward currents under voltage clamp at −80 mV. Representative examples are illustrated in Fig. 6*A* and mean data, normalized to cell size, is shown in Fig. 6*B*. Inward currents in response to a K^+ puff were nearly twice the amplitude in the ventral horn when compared with the dorsal horn. In both regions, this response was almost completely eliminated in Ba^{2+} (not shown). As a means to quantify this data, we integrated the area under the curve before and after Ba^{2+} application. The subtracted area represents the Ba^{2+}-sensitive charge flow, i.e., K^+ ions fluxing through Kir channels during the pulse. These data were then normalized to whole cell capacitance to yield specific K^+ flow/unit membrane. Mean data from 10 ventral horn and 5 dorsal horn cells examined this way are illustrated in Fig. 6*B*. These data demonstrate that on average, equal K^+ challenges resulted in a 60% smaller K^+ ion influx in the dorsal horn as compared with the ventral horn (31.9 ± 6.3 pC/pF, $n = 10$, and 11.9 ± 2.3 $n = 5$ pC/pF, respectively, $P = 0.049$). Taken together, these data suggest regional differences in astrocytic Kir4.1 expression leads to a differential ability to respond to extracellular $[K^+]$.

DISCUSSION

Buffering of extracellular K^+ is widely believed to be an important homeostatic task performed by glial cells. A great deal of evidence suggests K^+ uptake into glial cells occurs through inwardly rectifying K^+ channels (Kir) and recent knockout studies (Kofuji et al. 2000; Neusch et al. 2006; Olsen et al. 2006) suggest Kir 4.1 is important for K^+ homeostasis. A high open probability at rest (P_o ~ 0.9, (Ransom and Sontheimer 1995) and an increased conductance with increased extracellular K^+ make Kir4.1 an ideal pathway for K^+ clearance. In this study, we demonstrate that astrocytes from two different regions of the spinal cord, regions that have clear distinctions in terms of function, vary in regard to Kir4.1 channel expression. Our immunohistochemical studies demonstrate highest Kir4.1 expression in the ventral lateral edge of the ventral horn (Rexed Laminae 9) and show decreasing expression as toward the superficial layers of the spinal cord (Rexed Laminae I/II). Western blots confirm our immunohistochemical results demonstrating enhanced expression of Kir4.1 in the ventral horn of the spinal cord. Importantly, our recordings from astrocytes in acute spinal cord slices confirm this difference is reflected in function, i.e., a more than twofold difference in the magnitude of Ba^{2+}-sensitive inwardly rectifying currents. This finding is significant as it correlates directly with, and may indeed explain previously observed differences in, extracellular K^+ homeostasis in these regions of the spinal cord. Specifically, in neonatal rat a single electrical stimulus to the dorsal root evokes significant increases in $[K+]_o$ in the dorsal horn, whereas the same stimulus fails to produce noticeable $[K^+]_o$ changes in the ventral horn (Walton and Chesler 1988). Furthermore, in the dorsal horn, a single orthodromic stimulation

caused $[K^+]_o$ increases by as much as 4 –5 mM. Additionally, baseline extracellular K^+ levels vary in this structure (Svoboda et al. 1988). Our data suggest this phenomenon may be directly explained by the reduced expression of Kir4.1 in astrocytes of the dorsal horn, and we show experimentally that these astrocytes have a significantly reduced ability to take up K^+. As in the preceding studies, our experiments were performed in neonatal animals, therefore it remains to be shown whether similar differences in Kir4.1 channel expression would be observed in adult animals. Importantly, the preceding findings were not due to overall differences in astrocyte number as GFAP expression did not differ between these regions. Astrocytic membrane as detected by GLT-1 staining on our Western blot appeared slightly higher in the dorsal horn of the spinal cord. Moreover, this difference in Kir current amplitude was not due to an overall reduction of K^+ channels in dorsal horn astrocytes as the relative expression of delayed rectifying and fast-inactivating K^+ channels was identical in astrocytes from both regions.

These differences in K^+ uptake may reflect differing demands on K^+ homeostasis in these two regions of the spinal cord, and hence Kir4.1 expression may simply be tuned to the relative demand for K^+ clearance. The ventral horn contains primarily motor pathways in which high-frequency electrical discharge is the norm. Hence K^+ release by motor neurons would be substantial. The dorsal horn, on the other hand, contains primarily sensory pathways many of which contain slowly conducting unmyelinated fibers with comparably slower discharge rates. It should be noted that Kir4.1 is not the only protein showing regionally differing expression within the spinal cord. Aquaporin1 (Oshio et al. 2006), Aquaporin4 (Nesic et al. 2006; Vitellaro-Zuccarello et al. 2005), GLT-1, and GLAST (Rothstein et al. 1994) are each differentially expressed, showing higher levels of expression in the superficial layers of the dorsal horn.

In addition to its role in K^+ clearance, Kir4.1 has been demonstrated to contribute to the negative resting membrane potential typical of most astrocytes. Astrocytes in which Kir4.1 is blocked with exogenously applied Ba^{2+} or astrocytes from Kir4.1 knock-out animals each rest at more depolarized potentials relative to normal astrocytes (Kofuji et al. 2000; Svoboda et al. 1988). A negative RMP is crucial for many transport systems operating in astrocytes including, glucose and neuro-transmitter transport. A more negative resting membrane potential translates in a greater Na^+ gradient across the membrane that is used as the energy source to drive these systems. Indeed, it was recently demonstrated that glutamate uptake in cultured cortical astrocytes decreased by >50% when cells were treated with siRNA to Kir4.1 (Kucheryavykh et al. 2007). In our study, astrocytes from the dorsal horn were slightly but significantly depolarized relative to ventral horn astrocytes. Hence glutamate uptake would be expected to be reduced unless cells showed a compensatory upregulation of transporter expression.

Recently, it was demonstrated that a progressive loss of Kir4.1 from astrocytes in the ventral horn parallels disease progression in an ALS mouse model (Kaiser et al. 2006). Moreover, when motor neurons were exposed to modest elevations in K^+ (10 mM) for 120 h, significant neuronal cell death occurred. The high expression of Kir4.1 in this region suggest that neurons from the ventral horn may be particularly sensitive to elevated extracellular K^+, and efficient clearance mechanisms are necessary for neuronal cell survival, again explaining the observed increases in Kir4.1 expression. In contrast, the reduced expression of Kir4.1 in the dorsal horn, the region of the spinal cord responsible for pain perception, may be of functional significance. Here it may indeed be beneficial to have a less effective system for K^+ clearance, which allows K^+ to increase during a painful or noxious stimulus. The increased K^+ load resulting from increased “painful” neuronal activity in this region may amplify the signal by slightly depolarizing neurons in this region, hence, increasing their firing frequency proportional to the nociceptive stimulus. Prolonged subtle increases in K^+ have been reported that are suggestive of lessened K^+ regulation in the dorsal horn. In a recent study, after being applied to the hind

paw of rats, it was demonstrated a sustained increase in $[K^+]_o$, by ≤3 mM above baseline, in the lower dorsal horn that persisted for >2 h (Svoboda et al. 1988). This elevation was due to self-sustained neuronal firing induced by the injury. This $[K^+]_o$ increase was graded with the intensity of the nociceptive stimulus. Clearly, these experiments demonstrate the spinal cord may indeed be a highly specialized structure regarding neuronal transmission and the physiological relevance of K^+ homeostasis warrants further examination in this regard.

Acknowledgements

We thank A. Margolies for technical expertise.

GRANTS

This work was supported by National Institute of Neurological Disorders and Stroke Grants RO1-NS-36692 and RO1-NS-31234.

References

Amedee T, Robert A, Coles JA. Potassium homeostasis and glial energy metabolism. Glia 1997;21:46–55. [PubMed: 9298846]

Bringmann A, Biedermann B, Reichenbach A. Expression of potassium channels during postnatal differentiation of rabbit Muller glial cells. Eur J Neurosci 1999;11:2883–2896. [PubMed: 10457185]

D'Ambrosio R, Gordon DS, Winn HR. Differential role of KIR channel and Na(+)/K(+)-pump in the regulation of extracellular K(+) in rat hippocampus. J Neurophysiol 2002;87:87–102. [PubMed: 11784732]

Frankenhauser B, Hodgkin AL. The after-effects of impulses in the giant nerve fibers of *Loligo*. J Physiol 1956;131:341–376. [PubMed: 13320339]

Hagiwara S, Takahashi K. The anomalous rectification and cation selectivity of the membrane of a starfish egg cell. J Membr Biol 1974;18:61–80. [PubMed: 4854650]

Jendelova P, Sykova E. Role of glia in K^+ and pH homeostasis in the neonatal rat spinal cord. Glia 1991;4:56–63. [PubMed: 1828787]

Kaiser M, Maletzki I, Hulsmann S, Holtmann B, Schulz-Schaeffer W, Kirchhoff F, Bahr M, Neusch C. Progressive loss of a glial potassium channel (KCNJ10) in the spinal cord of the SOD1 (G93A) transgenic mouse model of amyotrophic lateral sclerosis. J Neurochem 2006;99:900–912. [PubMed: 16925593]

Kofuji P, Ceelen P, Zahs KR, Surbeck LW, Lester HA, Newman EA. Genetic inactivation of an inwardly rectifying potassium channel (Kir4.1 subunit) in mice: phenotypic impact in retina. J Neurosci 2000;20:5733–5740. [PubMed: 10908613]

Kofuji P, Newman EA. Potassium buffering in the central nervous system. Neuroscience 2004;129:1043–1054.

Kucheryavykh YV, Kucheryavykh LY, Nichols CG, Maldonado HM, Baksi K, Reichenbach A, Skatchkov SN, Eaton MJ. Downregulation of Kir4.1 inward rectifying potassium channel subunits by RNAi impairs potassium transfer and glutamate uptake by cultured cortical astrocytes. Glia 2007;55:274–281. [PubMed: 17091490]

MacVicar BA, Feighan D, Brown A, Ransom B. Intrinsic optical signals in the rat optic nerve: role for K(+) uptake via NKCC1 and swelling of astrocytes. Glia 2002;37:114–123. [PubMed: 11754210]

Martin-Caraballo M, Dryer SE. Activity- and target-dependent regulation of large-conductance Ca^{2+}-activated K^+ channels in developing chick lumbar motoneurons. J Neurosci 2002;22:73–81. [PubMed: 11756490]

Nesic O, Lee J, Ye Z, Unabia GC, Rafati D, Hulsebosch CE, Perez-Polo JR. Acute and chronic changes in aquaporin 4 expression after spinal cord injury. Neuroscience 2006;143:779–792. [PubMed: 17074445]

Neusch C, Papadopoulos N, Muller M, Maletzki I, Winter SM, Hirrlinger J, Handschuh M, Bahr M, Richter DW, Kirchhoff F, Hulsmann S. Lack of the Kir4.1 channel subunit abolishes K^+ buffering

properties of astrocytes in the ventral respiratory group: impact on extracellular K^+ regulation. J Neurophysiol 2006;95:1843–1852. [PubMed: 16306174]

Newman EA. Inward-rectifying potassium channels in retinal glial (Müller) cells. J Neurosci 1993;13:3333–3345. [PubMed: 8340811]

Olsen ML, Higashimori H, Campbell SL, Hablitz JJ, Sontheimer H. Functional expression of K(ir)4.1 channels in spinal cord astrocytes. Glia 2006;53:516–528. [PubMed: 16369934]

Oshio K, Watanabe H, Yan D, Verkman AS, Manley GT. Impaired pain sensation in mice lacking Aquaporin-1 water channels. Biochem Biophys Res Commun 2006;341:1022–1028. [PubMed: 16476579]

Poopalasundaram S, Knott C, Shamotienko OG, Foran PG, Dolly JO, Ghiani CA, Gallo V, Wilkin GP. Glial heterogeneity in expression of the inwardly rectifying K^+ channel, Kir4.1, in adult rat CNS. Glia 2000;30:362–372. [PubMed: 10797616]

Ransom CB, Ransom BR, Sontheimer H. Activity-dependent K^+ accumulation in the rat optic nerve is cleared by temperature-sensitive and temperature-insensitive mechanisms. Soc Neurosci Abstr 1995;21.1

Ransom CB, Sontheimer H. Biophysical and pharmacological characterization of inwardly rectifying K^+ currents in rat spinal cord astrocytes. J Neurophysiol 1995;73:333–345. [PubMed: 7714576]

Rothstein JD, Martin L, Levey AI, Dykes-Hoberg M, Jin L, Wu D, Nash N, Kuncl RW. Localization of neuronal and glial glutamate transporters. Neuron 1994;13:713–725. [PubMed: 7917301]

Sakmann B, Trube G. Conductance properties of single inwardly rectifying potassium channels in ventricular cells from guinea-pig heart. J Physiol 1984;347:641–657. [PubMed: 6323703]

Schools GP, Zhou M, Kimelberg HK. Development of gap junctions in hippocampal astrocytes: evidence that whole cell electrophysiological phenotype is an intrinsic property of the individual cell. J Neurophysiol 2006;96:1383–1392. [PubMed: 16775204]

Sontheimer H, Trotter J, Schachner M, Kettenmann H. Channel expression correlates with differentiation stage during development of oligodendrocytes from their precursor cells in culture. Neuron 1989;2:1135–1145. [PubMed: 2560386]

Svoboda J, Motin V, Hajek I, Sykova E. Increase in extracellular potassium level in rat spinal dorsal horn induced by noxious stimulation and peripheral injury. Brain Res 1988;458:97–105. [PubMed: 3208102]

Sykova E. Extracellular K^+ accumulation in the central nervous system. Prog Biophys Mol Biol 1983;42:135–189. [PubMed: 6139844]

Van Harreveld A, Malhotra SK. Extracellular space in the cerebral cortex of the mouse. J Anat 1967;101:2–207.

Vitellaro-Zuccarello L, Mazzetti S, Bosisio P, Monti C, De Biasi S. Distribution of Aquaporin 4 in rodent spinal cord: relationship with astrocyte markers and chondroitin sulfate proteoglycans. Glia 2005;51:148–159. [PubMed: 15789430]

Walton KD, Chesler M. Activity-related extracellular potassium transients in the neonatal rat spinal cord: an in vitro study. Neuroscience 1988;25:983–995. [PubMed: 2457188]

Walz W. Role of astrocytes in the clearance of excess extracellular potassium. Neurochem Int 2000;36:291–300. [PubMed: 10732996]

Williamson AV, Compston DAS, Randall AD. Analysis of the ion channel complement of the rat oligodendrocyte progenitor in a commonly studied in vitro preparation. Eur J Neurosci 1997;9:706–720. [PubMed: 9153577]

Xiong ZQ, Stringer JL. Astrocytic regulation of the recovery of extracellular potassium after seizures in vivo. Eur J Neurosci 1999;11:1677–1684. [PubMed: 10215921]

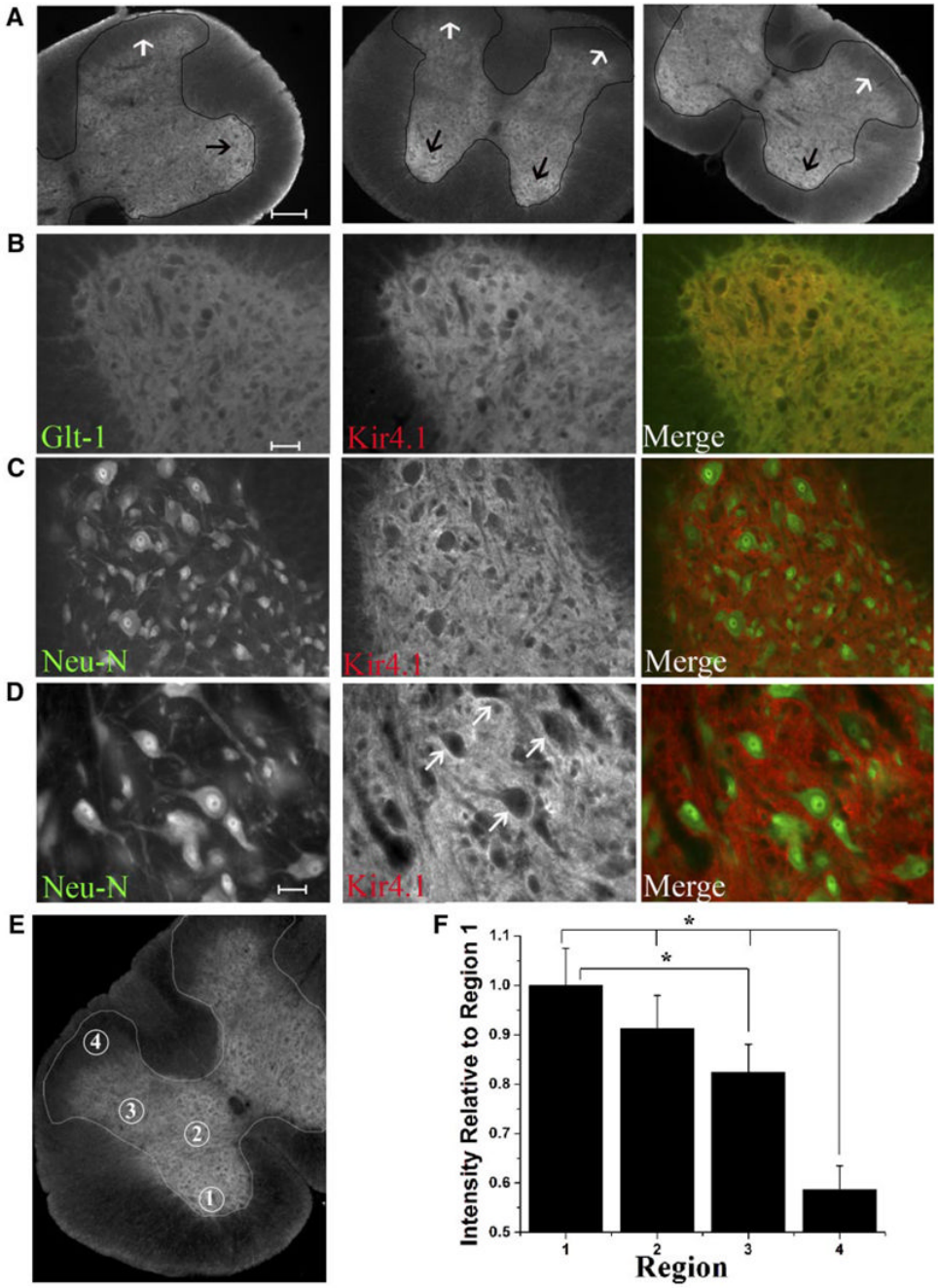

Fig. 1.

Immunohistochemistry demonstrates highest Kir4.1 staining in the ventral horn with very low immunoreactivity in the apex of the dorsal horn. *A*: low-magnification images from different regions of the spinal cord demonstrate highest Kir4.1 immunoreactivity in the ventral horn and very little staining visible in the dorsal horn of the spinal cord. The gray matter is lightly outlined in black for visualization. The black arrows indicate the ventral horn, the region of the cord that labels most intensely for Kir4.1. The white arrows indicate the superficial layers of the dorsal horn which demonstrates little Kir4.1 immunoreactivity. *B*: images from the ventral horn demonstrating Kir 4.1 largely overlapped with GLT-1 as demonstrated by the yellow color in the merged image. *C*: Kir4.1 and Neu-N labeling appear distinct in the ventral horn.

D: high-magnification images from the ventral horn demonstrate Kir4.1 staining is most intense surrounding neuronal cell bodies. (Scale bars *A*, 200 μm, *B* and *C*, 100 μm, *G*, 50 μm). *E*: circled regions in this image correspond to Rexed's Laminae IX (region1), Rexed's Laminae VII (region 2), Rexed's Laminae V (region 3), and Rexed's Laminae I/II (region 4); regions that were used for relative quantification of Kir4.1 expression in low-magnification images of transverse sections in the spinal cord. *F*: qauntification of Kir4.1 expression in transverse sections of the spinal cord reveal significant differences in Kir4.1 expression in Rexed's Laminae IV, VII, V, I/II. Mean data demonstrates significant differences between Rexed's Laminae 1/II and all other regions of the spinal cord examined ($P < 0.001$, Tukey-Kramer multiple comparisons test, $n = 21$). Kir 4.1 expression in region 3 or Rexed's Laminae V is also significantly different from Rexed's Laminae 9 ($n = 21$, $P < 0.001$).

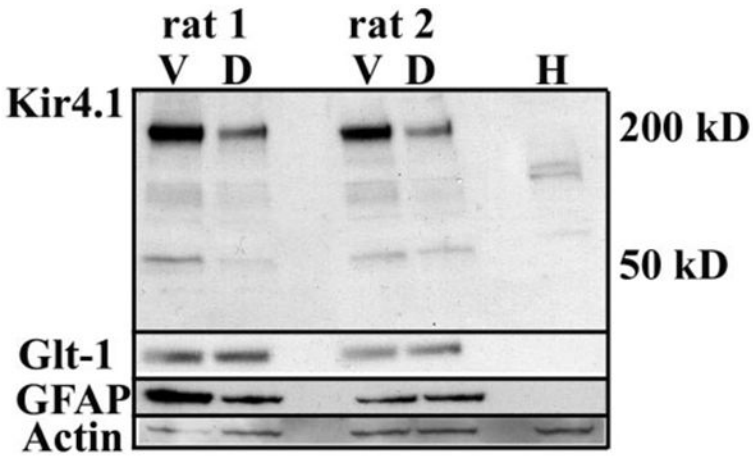

Fig. 2.

Western blot demonstrates Kir4.1 expression is significantly higher in the ventral horn compared with the dorsal horn. This blot contains dorsal and ventral gray matter lysates from 2 different animals probed for Kir4.1. A prominent band was detected at ~200 kD that corresponds to a tetramer and a band at ~50 kD (a monomer) was detected. For comparison and to evaluate astrocyte total protein, this blot was re-probed with antibodies to GLT-1, and GFAP. For a loading control, this blot was probed with actin. We presume the band at ~100 kD to be nonspecific binding as it is also present in the human embryonic kidney (HEK) cell lane, a cell line that does not express Kir4.1.

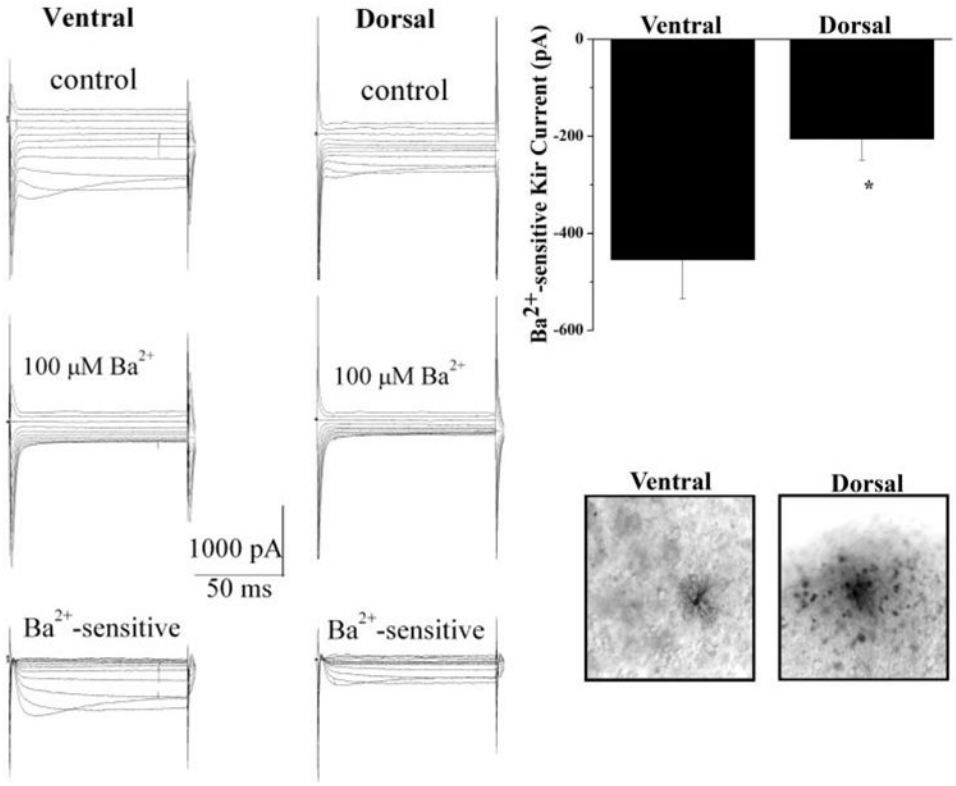

Fig. 3.

Whole cell patch-clamp recording from acute spinal cord slices reveals a significant difference in Kir current amplitude between the two regions of the spinal cord. *A*: typical voltage step response (protocol shown in *inset*) from ventral and dorsal horn astrocytes show Kir currents in the 2 regions share similar properties (inactivation at hyperpolarized potentials and complete inactivation in 100 μm Ba^{2+}); however, Ba^{2+}-sensitive Kir currents in the ventral horn are ~2-fold larger. *B*: mean data demonstrate a significant difference in Ba^{2+}-sensitive Kir currents (at −140 mV) in astrocytes from the ventral horn and dorsal horn (−453.8 ± 81.4, pA n = 25, and −205.3 ± 44.2 pA, n = 21, P = 0.0110, respectively). *C*: representative examples of filled cells from the ventral and dorsal regions of the spinal cord are shown.

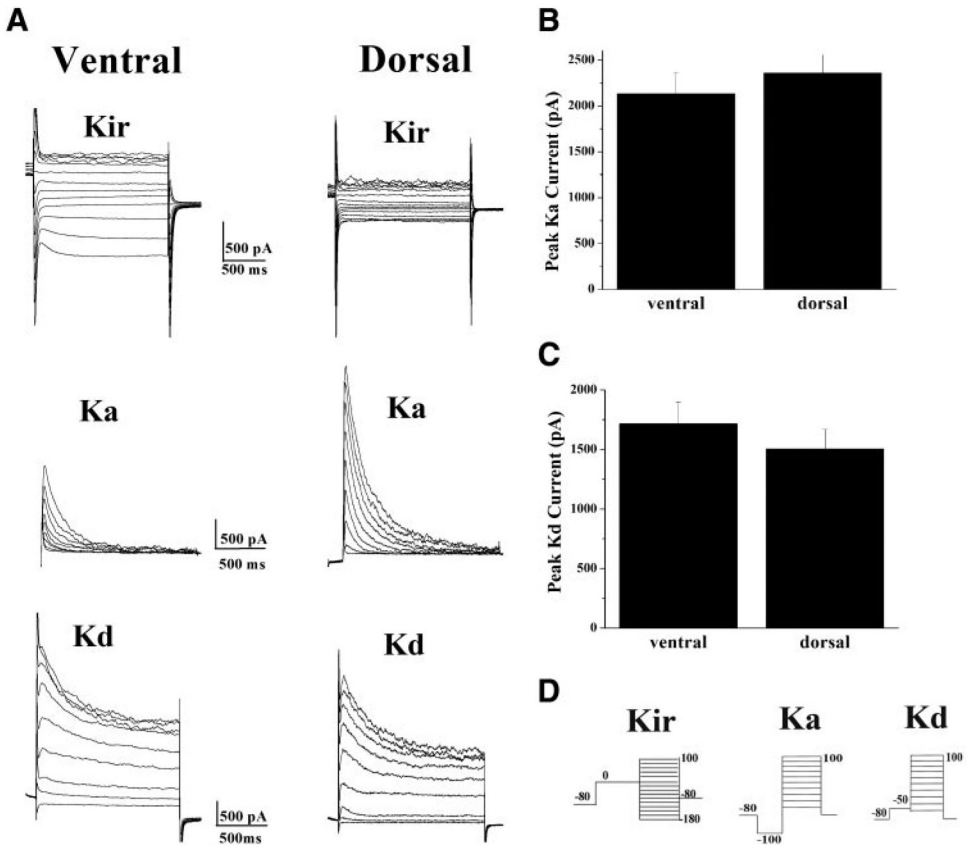

Fig. 4.

There is no statistical difference in either fast-inactivating (Ka) or delayed-rectifier (Kd) potassium currents in the dorsal and ventral horn. *A*: representative examples of Kir, Ka, and Kd currents from astrocytes in the ventral and dorsal region of the spinal cord. Kir currents are consistently smaller in the dorsal horn, whereas Ka (*middle*) and Kd currents (*bottom*) in the 2 regions are variable. *B* and *C*: mean data reveals there is no statistical difference between Ka (2,132.3 ± 225.4 pA, ventral, $n = 33$, and 2,358.3 ± 199.7 pA, dorsal, $n = 31$) or Kd (1,714.3 ± 179.7 pA, ventral, $n = 33$, and 1,504.6 ± 161.5 pA, dorsal, $n = 31$) currents in the 2 regions. *D*: protocols used to isolate Kir, Ka, and Kd currents. The protocol used to activate Ka currents activates both Ka and Kd currents, therefore a point by point subtraction (Ka − Kd) is used to isolate Ka currents.

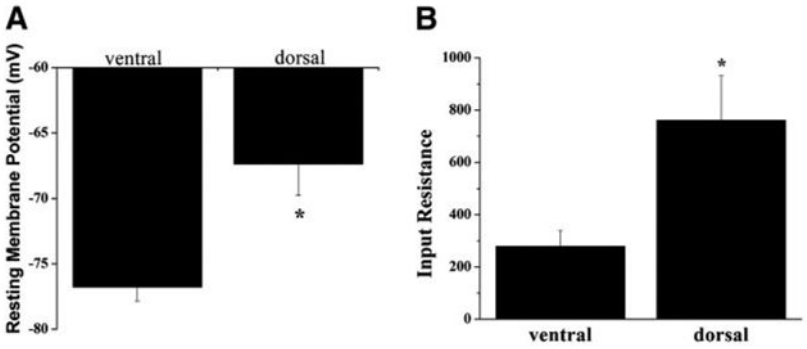

Fig. 5.

Astrocytes from the dorsal and ventral horn exhibit other electrophysiological differences. *A*: resting membrane potentials are significantly depolarized in the dorsal horn (−67.4 ± 2.4 mV, $n = 33$), relative to ventral horn astrocytes (−76.8 ± 1.1 mV, $n = 34$, $P = 0.0008$). *B*: input resistance of dorsal horn astrocytes is significantly higher in dorsal horn astrocytes when compared with astrocytes from the ventral horn (760.5 ± 171.9 mΩ, $n = 18$, and 279.1 ± 60.9 mΩ, $n = 18$, $P = 0.0153$, respectively).

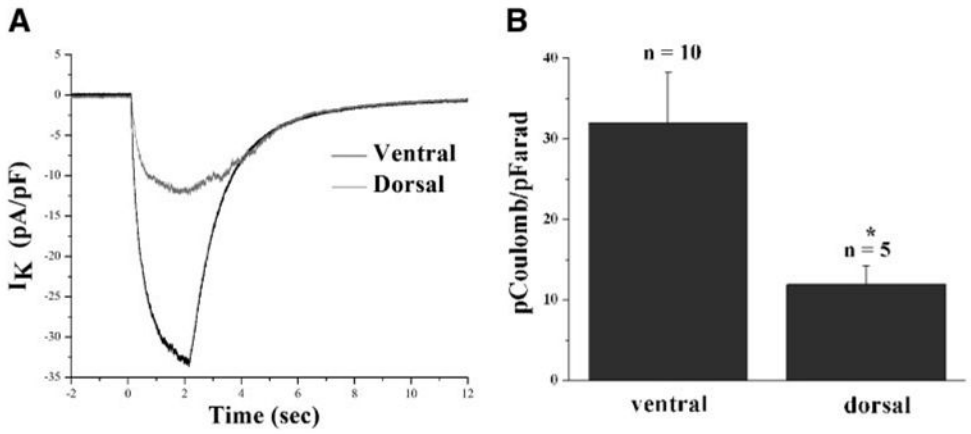

Fig. 6.

Consistent with a decreased ability to clear potassium, astrocytes from the dorsal horn exhibit a smaller response when exposed to increased potassium concentrations. *A*: typical response observed from voltage clamped (−80 mV) ventral and dorsal horn astrocytes when exposed to a 2-s puff of a high external potassium solution (130 mM). *B*: mean data were analyzed by subtracting the control trace from the trace after 100 μm Ba^{2+} and integrating this subtracted area. Data from several cells in each region show that cells in the dorsal horn exhibited a greater than twofold smaller response than cells from the ventral horn. The total Ba^{2+}-sensitive charge per unit membrane in the ventral horn was 31.91 ± 6.3 pC/pF, n = 10, whereas values in the dorsal horn measured 11.9 ± 2.3 pC/pF, n = 5.